Energy dependence of incomplete fusion processes in the $^{16}O+^{181}Ta$ system: Measurement and analysis of forward-recoil–range distributions at $E_{lab} \leqslant 7$ MeV/nucleon

Devendra P. Singh,[1,*] Unnati,[1] Pushpendra P. Singh,[2] Abhishek Yadav,[1] Manoj Kumar Sharma,[3] B. P. Singh,[1,†] K. S. Golda,[4] Rakesh Kumar,[4] A. K. Sinha,[5] and R. Prasad[1]

[1]*Department of Physics, Aligarh Muslim University, Aligarh (UP)-202 002, India*
[2]*INFN-Laboratori Nazionali di Legnaro, I-35020 Legnaro, Italy*
[3]*Department of Physics, S. V. College, Aligarh (UP)-202 001, India*
[4]*Inter-University Accelerator Center, Aruna Asaf Ali Marg, New Delhi-110 067, India*
[5]*UGC-DAE-CSR, Bidhan Nagar, Kolkata-700 098, India*

(Received 4 September 2009; revised manuscript received 7 April 2010; published 21 May 2010)

To study the energy dependence of incomplete fusion processes, the recoil range distributions for the reactions ^{181}Ta(^{16}O,xn), ^{181}Ta(^{16}O,pxn), ^{181}Ta(^{16}O,αn), ^{181}Ta(^{16}O,α2n), ^{181}Ta(^{16}O,α3n), and ^{181}Ta(^{16}O,2α3n) have been measured at ≈81-, 90-, and 96 MeV beam energies. The disentanglement of the complete and incomplete fusion processes have been done in terms of full and partial linear momentum transfer from the projectile to the target nucleus. The measurements have been done using recoil catcher technique. The experimentally measured forward recoil range distributions have been interpreted in terms of breakup fusion model. Detailed analysis of the data indicates that incomplete fusion processes have significant contribution at energies as low as ≈5 MeV/nucleon and their contribution is found to increase with energy.

DOI: 10.1103/PhysRevC.81.054607 PACS number(s): 25.70.Mn, 25.70.Gh, 25.70.Jj

I. INTRODUCTION

The study of the dynamics of heavy-ion (HI) collisions involving asymmetric nuclei at energies around the Coulomb barrier (CB) has been a topic of interest in recent years. In recent experiments [1–5], heavy residues populated by complete fusion (CF) with full momentum transfer and from incomplete fusion (ICF) with partial momentum transfer have been identified. Each of these processes leads to the characteristic velocity distribution of the reaction products. As such, the measured yield of a particular isotope as a function of velocity or rather the range of residues in a stopping medium helps to identify the origin of the observed reaction products. The incomplete momentum transfer events referred to as ICF reactions [6,7] can be understood on the basis of disappearance of pocket in the one-dimensional internuclear potential energy as the angular momentum increases. To reduce the effective angular momentum of the composite nucleus (CN) and to restore a pocket in the internuclear potential energy, as the entrance channel angular momentum is increased, an increasing factor of the projectile may escape and carries away some of the angular momentum. Because a portion of the projectile is not captured by the target, there is a deficit in the linear momentum of CN, when compared with the projectile momentum. An incomplete linear momentum transfer (LMT) event may be observed directly from the measurement of the velocity/range distribution [8–10] of the residues. The model of Siwek-Wilczynska [6,11] assumes that the maximum angular momentum (ℓ_{crit}), associated with complete LMT, is given by the disappearance of pocket in the one-dimensional internuclear potential energy and does not take into account angular momentum dissipation in the entrance channel. Because of the localization of this process in ℓ space, there is a strong correlation between the captured mass and the angular momentum/excitation energy of the heavy residue. This prediction lay at the root of the angular momentum dependence of the ICF reactions [11].

Though the ICF reactions have been extensively studied [12–14], nevertheless, no clear picture of the reaction dynamics has followed. With a view to understand various ICF processes, a variety of dynamical models/theories, like the Break-Up Fusion (BUF) model [15], Hot-Spot model [16], Promptly Emitted Particle (PEP) model [17–20], the EXCITON model [21], SUMRULE model [22], etc., have been proposed to explain ICF reaction dynamics. It may be pointed out that although these models predict the ICF reaction cross section at $E \geqslant 10$ MeV/nucleon, none of these models is suitable to predict the ICF processes at energies ≈5–7 MeV/nucleon. At present, it is well recognized [1,23–27] that the ICF reactions begin with the CF reactions at moderate energies. Some of the recent studies [28–32] showed the onset of ICF processes just above the CB. Several extensive studies [4,23,29–39] based on excitation function (EF) and recoil range distribution (RRD) measurements are available. However, the energy dependence of ICF reactions is still lacking. In the present work, to understand the ICF reaction dynamics and to study its energy dependence, the RRDs of the CF and ICF products in the $^{16}O+^{181}Ta$ system at the beam energies ≈81, 90, and 96 MeV have been measured. The present work is in continuation to our recent investigation [40] on the same system, where the measurement and analysis of excitation functions has been used to investigate the role of break-up processes. A detailed description of the experimental setup, etc. is already presented [40], however, for the sake of completeness a brief description

*dpsingh19@gmail.com
†bpsinghamu@gmail.com

of the experimental methodology is given in Sec. II. The details of the measurement of RRDs are described in Sec. III and finally the conclusions drawn from this study are presented in Sec. IV.

II. EXPERIMENTAL DETAILS

The experiments have been performed, using energetic $^{16}O^{7+}$ ion beams delivered from the 15UD-Pelletron accelerator of the Inter-University Accelerator Center (IUAC), New Delhi, India. Although the methodological details are somewhat similar to those already given in our earlier works [32,40], for quick reference, a brief description of sample preparation, irradiations, postirradiation analysis, etc. is given here.

In the present work, the isotopically pure sample of ^{181}Ta (abundance =100%) of thickness ≈150 μg/cm^2 has been deposited by the electro-deposition technique on Al foils of thickness ≈1.1–1.5 mg/cm^2. The thicknesses of the samples have been determined by the α-transmission method. The samples have been pasted on rectangular Al holders having concentric holes of 1.0-cm diameter. The irradiations have been performed using an $^{16}O^{7+}$ beam in the general purpose scattering chamber (GPSC), which has an invacuum transfer facility (ITF). In each irradiation, stacks of thin Al-catcher foils (with the total thickness sufficient to stop CN formed via full LMT) have been placed just after the target, so that the heavy (slow) residues populated via CF and/or ICF could be trapped at various catcher foil thicknesses. The target ^{181}Ta has been mounted in such a way that the Al backing first faces the beam so that the recoiling nuclei, if any, of very short range, does not stop in the target thickness itself. The beam energies provided by accelerator, in three separate irradiations were 85, 94, and 100 MeV, so that after an energy loss of ≈3.7, 3.9, and 3.5 MeV in the target backing, the incident energies on the targets are estimated to be, respectively, 81.3, 90.1, and 96.5 MeV. The irradiations have been carried out for the duration of ≈12 h, with a beam current ≈7 pnA.

After irradiation, the stacks of the samples as well as Al catchers were taken out of GPSC using an ITF. The activities produced in each Al-catcher foil of the stacks were counted separately using a high-purity germanium (HPGe) spectrometer of 100 c.c. active volume coupled with the CAMAC-based FREEDOM [41] software. The spectrometer was precalibrated both for energy and efficiency using standard γ sources like ^{60}Co and ^{152}Eu. The resolution of the γ spectrometer was found to be ≈2 keV, for 1.33 MeV γ ray of the ^{60}Co source, during the counting of the samples. A list of the radionuclides populated in the ^{16}O+^{181}Ta system, the energy of identified γ rays used for the decay-curve analysis, along with their branching ratios are given in our earlier work on the same system [40]. The evaporation residues (ERs) populated via CF and/or ICF are supposed to be trapped at different catcher foil thicknesses, depending on the recoil velocity and/or the degree of LMT of projectile associated with the mode of formation. The γ-ray spectra of each foil have been recorded at increasing times so that the decay-curve analysis can be done to verify the half-lives and identification of the residues. The measured half-lives of the residues were found to be in good agreement with the literature values [42]. A FORTRAN program EXPSIGMA based on the standard formulation [43] has been used for the determination of the production yield of evaporation residues in different catcher foils.

In the present work, the production probabilities of ^{194}Tl(3n), ^{193}Tl^g(4n), ^{192}Tl(5n), ^{193}Hg^{g,m}(p3n), ^{192}Hg(p4n), ^{191}Hg^{g,m}(p5n), ^{192}Au^g(αn), ^{191}Au^g(α2n), ^{190}Au^g(α3n), and ^{186}Ir^g(2α3n) nuclides produced in the ^{16}O+^{181}Ta system have been measured at different catcher foil thicknesses to estimate the RRDs. In general, a residue populated via a specific channel, often emits several γ rays of different energies. The cross section for a channel has been determined from the measured intensities of several characteristic γ rays and the final value is taken as the weighted average of cross sections obtained for these γ rays [44]. The production yield of different reaction products has been deduced by normalizing the experimentally measured production cross sections with the respective catcher foil thicknesses. To generate RRDs, the normalized yield of an individual reaction product has been plotted as a function of cumulative catcher foil thicknesses. The sources of uncertainty are already described in Ref. [40].

III. ANALYSIS OF FORWARD RECOIL RANGE DISTRIBUTIONS

The degree of the linear momentum transfer (ρ_{LMT}) from the projectile to the target nucleus is the basis of recoil velocity of the reaction products, which may be used to differentiate the CF and ICF processes. As already mentioned, ρ_{LMT} is proportional to the fused mass of the projectile (i.e., maximum LMT gives rise to maximum recoil velocity to the reaction product). In the CF process, the maximum ρ_{LMT} from the projectile to the target nucleus is expected. For a given entrance channel the CN has predetermined mass, energy, and linear momentum. In case of ICF, partial ρ_{LMT} leads to the formation of an incompletely fused composite system in excited state. For an incompletely fused composite system, the following quantities viz., mass, energy, and momenta of CN may not have unique values. This may be because of the fluctuations in the fused mass from the projectile to the target nucleus. The experimentally measured forward recoil ranges of final reaction products in the stopping medium may give an indication of the ρ_{LMT} involved. As such, the radio-nuclides populated via a lower degree of LMT, show relatively smaller depth (momentum transfer component) in the stopping medium as compared to the entire LMT populations. For a different ρ_{LMT}, the residues may have different recoil ranges in the stopping medium. Therefore, the forward recoil range distributions may be used as a probe to investigate the partial fusion of the projectile in ICF processes. The normalized yields of different reaction products have been generated for the residues viz., ^{194}Tl, ^{193}Tl, ^{192}Tl, ^{193}Hg^g, ^{193}Hg^m, ^{192}Hg, ^{191}Hg^g, ^{191}Hg^m, ^{192}Au^g, ^{191}Au^g, ^{190}Au^g, and ^{186}Ir^g and plotted as a function of cumulative catcher thickness. As a representative case to show different ρ_{LMT} components in various CF and ICF processes the RRDs for ^{192}Hg(p4n), ^{191}Au^g(α2n), and ^{186}Ir^g(2α3n) residues have been presented in Figs. 1–3, at three different beam energies each. The size of

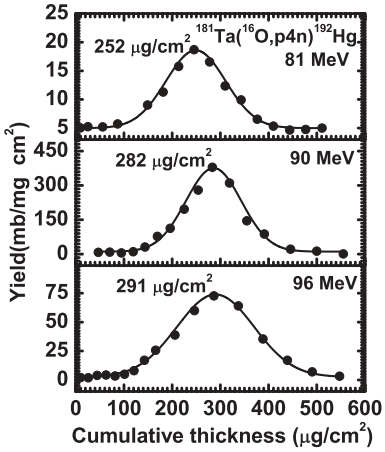

FIG. 1. Experimentally measured forward recoil range distributions for ^{192}Hg($p4n$) at projectile energies at ≈81, 90, and 96 MeV.

the circles, in Figs. 1–3, includes the uncertainty in the yield values. As can be seen from these figures, the measured RRDs clearly indicate the different momentum transfer components, depending on the fused mass of the projectile with the target nucleus.

In case of the $p4n$ channel (Fig. 1), the measured RRDs show only a single peak, at all the three bombarding energies, indicating only single linear momentum transfer component (a characteristic of the CF process) involved in the production of ^{192}Hg. A close observation of the range distribution of ^{192}Hg (Fig. 1) reveals that FRRDs peak at relatively higher cumulative catcher thickness as the beam energy increases. It is simply because the LMT increases with beam energy. Further, it may be pointed out that, the neutron emission from the recoiling nuclei may change the energy/momentum of the recoiling nucleus, depending on the direction of emission. This may be reflected in the width (FWHM) of the experimentally measured recoil range distributions. The width may also arise because of the contribution from straggling effects. The identified reaction products and their experimentally measured most probable FRRDs, $R_{p(\mathrm{exp})}$, for all the CF residues along

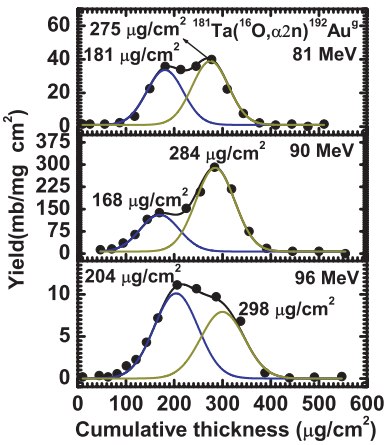

FIG. 2. (Color online) Experimentally measured forward recoil range distributions for ^{191g}Au($\alpha 2n$) at projectile energies ≈81, 90, and 96 MeV.

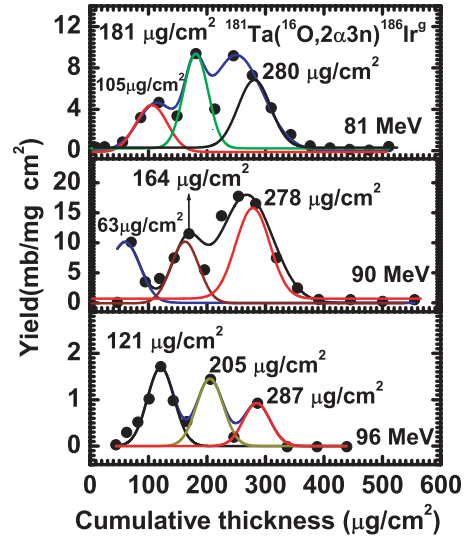

FIG. 3. (Color online) Experimentally measured forward recoil range distributions for ^{186g}Ir($2\alpha 3n$) at projectile energies ≈81, 90, and 96 MeV.

with the theoretically estimated (using the code SRIM [45]) mean ranges $R_{p(\mathrm{the})}$, are given in Table I. The most probable recoil ranges have been theoretically calculated, assuming that in the case of CF, the incoming ion completely fuses with the target nucleus and transfers its total linear momentum to the fused system, which recoils to conserve the input linear momentum. On the basis of the previous description, it may be mentioned that the population of reaction products ^{192}Hg populated via $p4n$ channel is associated with the entire LMT from projectile to the target nucleus, and may be represented as

$$^{16}\mathrm{O} + {}^{181}\mathrm{Ta} \longrightarrow {}^{197}\mathrm{Tl}^{*} \longrightarrow {}^{192}\mathrm{Hg} + p4n.$$

In the similar fashion, the RRDs for the residues ^{194}Tl, ^{193}Tl, ^{192}Tl, ^{193}Hg^{g}, ^{193}Hg^{m}, ^{191}Hg^{g}, and ^{191}Hg^{m} are found to have single peak associated with complete linear momentum transfer from projectile to the composite nucleus, indicating their production via the CF process only.

Further, in case of reaction channels (αn), ($\alpha 2n$), and ($\alpha 3n$). where the residues ^{192}Au^{g}, ^{191}Au^{g}, and ^{190}Au^{g} are populated, each of the FRRDs are found to have a two-peak structure. The observed FRRDs were resolved into two peaks, with the Gaussian peak-fitting option of the ORIGIN software, one corresponding to the complete momentum transfer events and the other corresponding to the fusion of ^{12}C (if ^{16}O breaks into $^{12}\mathrm{C} + \alpha$ and ^{12}C fuses) with ^{181}Ta. As a representative case, the FRRDs for the residues, ^{191}Au^{g}, have been plotted at three different energies and are shown in Fig. 2. As can be seen from this figure, the FRRDs in this case may be resolved into two Gaussian peaks (also in case of all other αxn channels), indicating the presence of more than one linear momentum transfer components, one associated with the fusion of ^{16}O and the other due to the fusion of ^{12}C. From Fig. 2, it may be observed that for the residues ^{191}Au^{g}, there are two linear momentum transfer components, one having mean ranges at 275 ± 37, 284 ± 40, and 298 ± 45 μg/cm^2 at ≈81, 90, and 96 MeV beam energies (indicating fusion of ^{16}O) and at 181 ± 37,

TABLE I. Experimentally measured forward recoil ranges $R_{p(\mathrm{exp})}$ deduced from RRD curves, and theoretically calculated most probable mean ranges $R_{p(\mathrm{the})}$ for CF components at ≈81, 90, and 96 MeV, using the range energy relation [45] for the reaction products produced in the interaction of ^{16}O with ^{181}Ta.

Residues	Energy (E) ≈ 81 MeV		Energy (E) ≈ 90 MeV		Energy (E) ≈ 96 MeV	
	$R_{p(\mathrm{exp})}$ (μg/cm^2)	$R_{p(\mathrm{the})}$ (μg/cm^2)	$R_{p(\mathrm{exp})}$ (μg/cm^2)	$R_{p(\mathrm{the})}$ (μg/cm^2)	$R_{p(\mathrm{exp})}$ (μg/cm^2)	$R_{p(\mathrm{the})}$ (μg/cm^2)
^{194}Tl($3n$)	265 ± 76	267	275 ± 47	287	286 ± 48	298
^{193}Tl^g($4n$)	260 ± 77	267	254 ± 39	287	286 ± 67	298
^{192}Tl($5n$)	244 ± 58	267	255 ± 21	287	264 ± 75	298
^{193}Hg^g($p3n$)	261 ± 82	267	257 ± 75	287	290 ± 52	298
^{193}Hg^m($p3n$)	275 ± 75	267	270 ± 60	287	292 ± 51	298
^{192}Hg($p4n$)	252 ± 61	267	282 ± 57	287	291 ± 80	298
^{191}Hg^g($p5n$)	276 ± 47	267	256 ± 47	287	277 ± 50	298
^{191}Hg^m($p5n$)	249 ± 53	267	230 ± 65	287	287 ± 69	298

168 ± 40, and 204 ± 45 μg/cm^2 (indicating fusion of ^{12}C) at the respective three energies. It may also be observed from Fig. 2 that the peak value of the ranges, that is, $R_{p(\mathrm{exp})}$ shifts toward higher cumulative catcher thickness as the beam energy increases, as expected. It can be inferred that the residues ^{191}Au^g populated through ^{181}Ta(^{16}O,$\alpha 2n$) channel have the contributions from both the processes viz., CF and ICF. The residues ^{191}Au^g may be populated via CF and/or ICF channels i.e., via,

(a) Complete fusion of ^{16}O as

$$^{16}\mathrm{O} + {}^{181}\mathrm{Ta} \Longrightarrow {}^{197}\mathrm{Tl}^* \Longrightarrow {}^{191}\mathrm{Au}^{g*} + \alpha + 2n;$$

(b) Incomplete fusion of ^{16}O as

$$^{16}\mathrm{O}(^{12}\mathrm{C} + \alpha) + {}^{181}\mathrm{Ta} \underset{\text{(spectator)}}{\Longrightarrow} {}^{193}\mathrm{Au}^* + \alpha$$
$$^{193}\mathrm{Au}^* \Longrightarrow {}^{191}\mathrm{Au}^g + 2n.$$

The measured ranges for the channels (αn), ($\alpha 2n$), and ($\alpha 3n$) via the CF and ICF processes as mentioned previously are presented in Table II, and are found to agree reasonably well with those calculated using code SRIM, on the basis of the breakup fusion model. In these calculations, it is assumed that no energy is lost during the breakup of the incident ion. In these reactions, the α particle essentially acts as spectator during the reaction, so that linear momentum transfer of the residue is reduced to 3/4 of the CN value. Similarly, it may also be assumed that ^{16}O may break into four α fragments, two α particles may fuse with the target nucleus, and the remaining two may escape without any interaction. One such case has been observed in the present work where ^{186}Ir^g($T_{1/2}$ = 16.64 h), residues are produced via the $2\alpha 3n$ channel. The measured FRRDs for residues ^{186}Ir^g are shown in Fig. 3. As can be seen from this figure, the FRRDs may be resolved clearly into three Gaussian peaks, indicating the presence of more than one linear momentum transfer component associated with the

TABLE II. Experimentally measured $R_{p(\mathrm{exp})}$ deduced from RRD curves and theoretically calculated $R_{p(\mathrm{the})}$ for ICF components at ≈81, 90, and 96 MeV.

Residues	$R_{p(\mathrm{exp})}\mu$g/cm^2 (CF of ^{16}O)	$R_{p(\mathrm{the})}\mu$g/cm^2 (CF of ^{16}O)	$R_{p(\mathrm{exp})}\mu$g/cm^2 (ICF of ^{12}C)	$R_{p(\mathrm{the})}\mu$g/cm^2 (ICF of ^{12}C)	$R_{p(\mathrm{exp})}\mu$g/cm^2 (ICF of ^{8}Be)	$R_{p(\mathrm{the})}\mu$g/cm^2 (ICF of ^{8}Be)
Energy (E) ≈ 81 MeV						
^{192}Au^g(αn)	275 ± 45	267	145 ± 45	198	–	–
^{191}Au^g(α2n)	275 ± 37	267	181 ± 37	198	–	–
^{190}Au^g(α3n)	282 ± 45	267	181 ± 45	198	–	–
^{186}Ir^g(2α3n)	280 ± 30	267	181 ± 28	198	105 ± 30	108
Energy (E) ≈ 90 MeV						
^{192}Au^g(αn)	256 ± 43	287	168 ± 43	215	–	–
^{191}Au^g(α2n)	284 ± 40	287	168 ± 40	215	–	–
^{190}Au^g(α3n)	282 ± 32	287	196 ± 32	215	–	–
^{186}Ir^g(2α3n)	278 ± 28	287	164 ± 28	215	63 ± 28	117
Energy (E) ≈ 96 MeV						
^{192}Au^g(αn)	290 ± 55	298	200 ± 55	227	–	–
^{191}Au^g(α2n)	298 ± 45	298	204 ± 45	227	–	–
^{190}Au^g(α3n)	286 ± 55	298	213 ± 55	227	–	–
^{186}Ir^g(2α3n)	287 ± 23	298	205 ± 23	227	121 ± 23	122

CF of ^{16}O and ICF of ^{12}C and ^{8}Be. From this figure, it may be resolved that the population of ^{186}Ir^{g} residues, at the energies of interest, may take place via the three linear momentum transfer components. The peaks at ranges 280 ± 30, 278 ± 28, and 287 ± 23 μg/cm^2 at $\approx$81, 90, and 96 MeV energies, respectively, may be attributed to the fusion of ^{16}O. The ranges at 181 ± 28, 164 ± 28, and 205 ± 23 μg/cm^2 (fusion of ^{12}C) and 105 ± 30, 63 ± 28, and 121 ± 23 μg/cm^2 (fusion of ^{8}Be) at the respective energies have also been observed. As such, it can be inferred that the residues ^{186}Ir^{g} produced through ^{181}Ta(^{16}O, $2\alpha 3n$) reaction channel have the contribution from both the processes, namely, CF as well as ICF, which may be represented as attributable to:

(a) Complete fusion of ^{16}O, that is,

$$^{16}\mathrm{O} + {}^{181}\mathrm{Ta} \Longrightarrow {}^{197}\mathrm{Tl}^{*} \Longrightarrow {}^{186}\mathrm{Ir}^{g*} + 2\alpha + 3n;$$

(b) Incomplete fusion of ^{16}O, that is,

$$^{16}\mathrm{O}(^{12}\mathrm{C} + \alpha) + {}^{181}\mathrm{Ta} \underset{\text{(spectator)}}{\Longrightarrow} {}^{193}\mathrm{Au}^{*} + \alpha + 3n;$$

(c) Incomplete fusion of ^{16}O, that is,

$$^{16}\mathrm{O}(^{8}\mathrm{Be} + {}^{8}\mathrm{Be}) + {}^{181}\mathrm{Ta} \underset{\text{(spectator)}}{\Longrightarrow} {}^{189}\mathrm{Ir}^{*} + 2\alpha$$
$$^{189}\mathrm{Ir}^{*} \Longrightarrow {}^{186}\mathrm{Ir}^{g} + 3n.$$

In case of ICF, it is assumed that the incident ^{16}O ion breaks into fragments (e.g., ^{12}C and α or ^{8}Be and ^{8}Be) as it enters in the nuclear field of target nucleus. The fragments so produced are assumed to move with the velocity of the incident ion. One of the fragments (^{12}C or ^{8}Be or α) fuses with the target nucleus forming a composite system, which recoils in the forward direction to conserve the input linear momentum. It may be pointed out that the events due to fusion of single α particles have not been observed in the present work.

To study the energy dependence of CF (full LMT) and ICF (partial LMT) components, percentage relative contributions [32] of the CF and ICF components are deduced using the relation,

$$F_{\mathrm{ICF}} = \frac{\Sigma\sigma_{\mathrm{ICF}}}{\Sigma\sigma_{\mathrm{CF}} + \Sigma\sigma_{\mathrm{ICF}}} \times 100, \qquad (1)$$

where $\Sigma\sigma_{\mathrm{CF}}$ and $\Sigma\sigma_{\mathrm{ICF}}$ are the sum of cross sections (for all the measured xn, pxn, αxn, and $2\alpha xn$ channels obtained from the analysis of FRRDs) of CF and ICF processes, respectively.

The relative contribution of CF and ICF in the production of a particular reaction product may be computed by fitting the experimentally measured RRDs with Gaussian peaks using the ORIGIN software. The yield curves of evaporation residues obtained from RRDs are assumed to be Gaussian in nature and may be given as

$$Y = Y_0 + \frac{A}{\sqrt{2\pi\omega_A^2}} e^{-(R-R_P)^2/2\pi\omega_A^2}, \qquad (2)$$

where R_P is the most probable mean range, ω_A is the width parameter (FWHM) of the RRD, and A is the area under the peak.

The value of the χ^2 was minimized in the present analysis using a nonlinear least-square fit routine, keeping the width (ω_A) as constant at a given energy, and most probable mean range (R_P) has been kept at the peak position from the RRD data. Moreover, as indicated in Figs. 2 and 3, the residues show more than one RRD component. In such cases, the experimentally measured normalized yields have been fitted using the multipeak option in a similar way as mentioned previously. It may, however, be pointed out that choosing the width of Gaussian peak as a free parameter may influence the relative contributions derived from the figures. In the present work, the minimization of χ^2 and selected values of FWHM (kept as constant as shown in Table II) for the peak in complex RRD data were found to fit the experimental data satisfactorily. In the present work, an attempt has been made to disentangle the CF and ICF contributions by fitting the FRRD with Gaussian constrained at a range expected for full momentum transfer to estimate their relative contributions. The percentage ICF contributions of different fusion components have been obtained by dividing the area under the ICF peak of the corresponding fusion component by the total area associated with the experimental data employing Eq. (1). The values of F_{ICF} deduced from ICF data are plotted as a function of normalized beam energy (E_{beam}/CB) in Fig. 4. As can be seen from this figure that the ICF fraction increases with energy rapidly at lower energies, however, at relatively higher energies the F_{ICF} seems to move toward saturation. Furthermore, extrapolation of the curve in the lower energy region clearly indicates the onset of ICF processes even at energies very close to CB (i.e., from $\approx$5% above CB). It may be pointed out here that the F_{ICF} given in Fig. 4 presents the lower limit of incomplete fusion contributions as several other ICF channels could not be measured due to their short half-lives, and/or low intensity γ lines of the residues. It may not be out of place to mention that similar observations of ICF contributions increasing with energy and mass asymmetry have been obtained in several articles [9] by Morgenstern *et al.* However, their work involved measuring the velocity spectra employing the time-of-flight method in lighter systems and also at relatively higher energies of $\approx$10–25 MeV/n.

Furthermore, to understand the variation of CF and ICF contribution with energy in the individual reaction channels, the relative percentage contribution for CF and ICF processes

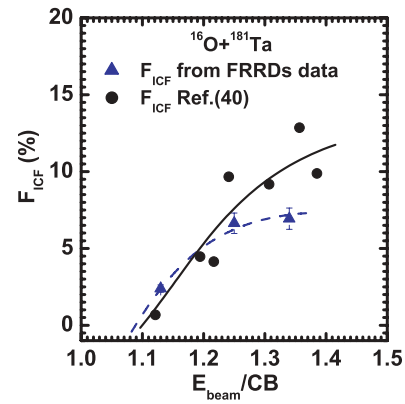

FIG. 4. (Color online) The percentage incomplete fusion fraction (F_{ICF}) deduced from the analysis of forward recoil range distributions as a function of normalized projectile energy. Data shown by triangle are obtained from the analysis of EFs [40].

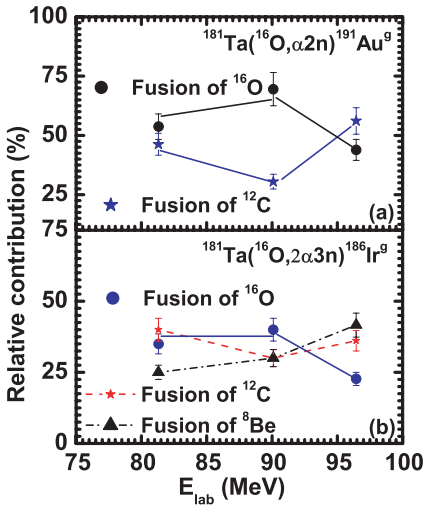

FIG. 5. (Color online) Relative strengths of the contributions coming from CF and ICF of ^{16}O with ^{181}Ta at projectile energies ≈81, 90, and 96 MeV for the production of residues ^{191g}Au($\alpha 2n$) and ^{186g}Ir($2\alpha 3n$). The lines joining data points are just to guide the eyes.

for $\alpha 2n$ and $2\alpha 3n$ are plotted as a function of laboratory beam energy as representative sets. One can be seen from Figs. 5(a) and 5(b) that as the energy increases from 81 to 90 MeV, the CF contribution remains almost constant within the uncertainty and then decreases at 96 MeV. Similarly, the fusion of ^{12}C appears to decrease and then increase at 96 MeV. However, the trend for ^{8}Be fusion contribution remains almost constant up to 90 MeV and then increases at 96 MeV beam energy. From Figs. 5(a) and 5(b), it may be observed that the relative ICF contribution for an individual channel may be as large as ≈50% at 96 MeV, however, the overall ICF contribution at this energy is around 7% only (Fig. 4). Moreover, as already mentioned, the RRDs for the residues ^{192,191,190}Au^{g} and ^{186}Ir^{g} also show peaks corresponding to the ICF of ^{12}C and/or ^{8}Be. The experimental ICF contributions for these residues could not be compared with theoretical values as there is no satisfactory model which can give ICF contributions. Furthermore, Fig. 6 shows the

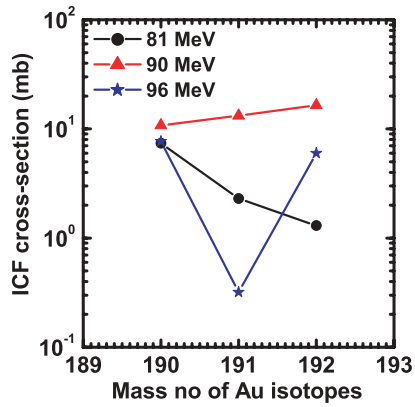

FIG. 6. (Color online) ICF contribution of different Au isotopes produced in the ^{16}O+^{181}Ta system at projectile energies ≈81, 90, and 96 MeV. The lines joining data points are just to guide the eyes.

ICF contributions of different Au isotopes at three different projectile energies. It may be observed from this figure that the production of ^{190}Au^{g} via ICF channel is nearly the same at 81, 90, and 96 MeV. However, the production probability of ^{191}Au^{g} is largest at 90 MeV and smallest at 96 MeV with some intermediate value at 81 MeV. Furthermore, a comparison of production probability of ^{190,191,192}Au^{g} at 81, 90, and 96 MeV indicates that maximum production of ^{192}Au^{g} is at 90 MeV and smallest at 81 MeV. However, at 96 MeV it has some intermediate value. The present data seem to be explained on the basis of the BUF model assuming that as the incident ion comes near the field of target nucleus, it may break up into its fragments and one of the fragments may fuse with the target nucleus, resulting finally into partial linear momentum transfer. The presently measured FRRD data clearly indicate that the momentum (mass) lost in the case of ICF processes at the time of interaction preferentially originates from the incident beam nuclei. A more detailed particle γ-coincidence experiment for this system (^{16}O+^{181}Ta) is proposed to have better insight into the reaction mechanism and the associated l values in the case of CF and ICF processes. The SUMRULE model calculation, carried out for the present system, which allow the ICF processes only for $l < l_{crit}$, underestimates the presently measured ICF cross-section data by a few orders of magnitude. As a typical example the experimentally measured cross sections for the ($\alpha 3n$) and ($2\alpha 3n$) channels are found to be ≈64.0 ± 9.6 mb and 5.0 ± 0.7 mb, however, the theoretically calculated SUMRULE values are 1.32×10^{-2} mb and 3.02×10^{-3} mb at 81 MeV beam energy. These discrepancies indicate the deviations from the assumptions of the model. Similar deviations have also been found by Parker *et al.* [1] in their study on the ^{12}C + ^{51}V system up to 100 MeV. The SUMRULE model assumes sharp cutoff l values for the CF and ICF processes. However, the present findings indicate a diffused boundary that may penetrate close to the barrier.

IV. CONCLUSIONS

The recoil range distributions for 13 residues—^{194}Tl, ^{193g}Tl, ^{192}Tl, ^{193}Hg^{g}, ^{193}Hg^{m}, ^{192}Hg, ^{191}Hg^{g}, ^{191}Hg^{m}, ^{192}Au^{g}, ^{191}Au^{g}, ^{190}Au^{g}, and ^{186}Ir^{g}—produced in the ^{16}O+^{181}Ta system at ≈81, 90, and 96 MeV beam energies have been measured. The measurement and analysis of the FRRDs of reaction products presented in this article strongly reveal a significant contribution from the partial LMT of the projectile associated with ICF in several α emitting channels. Different partial LMT components are attributed to the ^{12}C and/or ^{8}Be transfer from the ^{16}O projectile to the target nucleus. An attempt has also been made to obtain the relative contribution of CF and/or ICF components. The percentage ICF contributions are found to have an onset from ≈5% above CB. It has been found that, in general, the residues are not only populated via CF but ICF is also found to play an important role in the production of different reaction products involving direct α-cluster emission at these energies. However, in the case of ^{192}Au^{g}, ^{191}Au^{g}, ^{190}Au^{g}, and ^{186}Ir^{g} residues, the RRD data clearly indicate that the ICF reaction mechanism is dominant at the energies of interest in the present work. The results

obtained indicate that the forward recoil range distributions of the residues can be an extremely valuable information for establishing the CF and ICF yields at relatively low bombarding energies.

ACKNOWLEDGMENTS

The authors thank Prof. M. Zafar, Department of Physics, Aligarh Muslim University, Aligarh for providing all the necessary facilities. The authors are thankful to Prof. Amit Roy, Inter-University Accelerator Centre (IUAC), New Delhi, India for extending all the necessary facilities for performing the experiments and hospitality. We are also thankful to Dr. R. K. Bhowmik, R. P. Singh, and S. Muralithar for scientific discussions and support during the experiments. Thanks are also due to Mr. S. R. Abhilash for help in the target preparation. One of the authors (D.P.S.) thanks the UGC-DAE, Consortium for Scientific Research, Kolkata Centre, Kolkata, India, for providing financial support (Project No. CRS-076/AMU/P/RP/7409). R.P. and B.P.S. thank the Department of Science and Technology and University Grants Commission for support.

[1] D. J. Parker, J. Asher, T. W. Conlon, and N. Naquib, Phys. Rev. C **30**, 143 (1984).
[2] J. M. Alexander and L. Winsberg, Phys. Rev. **121**, 529 (1961).
[3] E. Gadioli *et al.*, Nucl. Phys. A **641**, 271 (1998).
[4] B. Bindu Kumar, S. Mukherjee, S. Chakrabarty, B. S. Tomar, A. Goswami, and S. B. Manohar, Phys. Rev. C **57**, 743 (1998).
[5] B. Bindu Kumar, A. Sharma, S. Mukherjee, S. Chakrabarty, P. K. Pujari, B. S. Tomar, A. Goswami, S. B. Manohar, and S. K. Datta, Phys. Rev. C **59**, 2923 (1999).
[6] K. Siwek-Wilczynska *et al.*, Phys. Rev. Lett. **42**, 1599 (1979).
[7] J. Wilczynski *et al.*, Phys. Rev. Lett. **45**, 606 (1980).
[8] J. R. Birkelund *et al.*, Bull. Am. Phys. Soc. **26**, 539 (1981).
[9] H. Morgenstern *et al.*, Phys. Lett. B **113**, 463 (1982); Phys. Rev. Lett. **52**, 1104 (1984).
[10] Y. Chan *et al.*, Phys. Rev. C **27**, 447 (1983).
[11] K. Siwek-Wilczynska, E. H. Du Marchie van Voorthuysen, J. van Popta, R. H. Siemssen, and J. Wilczynski, Nucl. Phys. A **330**, 150 (1979).
[12] H. C. Britt and A. R. Quinton, Phys. Rev. **124**, 877 (1961).
[13] S. E. Arnell *et al.*, Phys. Lett. B **129**, 23 (1983).
[14] H. W. Wilschut *et al.*, Phys. Lett. B **138**, 43 (1984).
[15] T. Udagawa *et al.*, Phys. Rev. Lett. **45**, 1311 (1980).
[16] R. Weiner *et al.*, Nucl. Phys. A **286**, 282 (1977).
[17] J. P. Bondrof *et al.*, Nucl. Phys. A **333**, 285 (1980).
[18] H. Tricoire *et al.*, Z. Phys. A **312**, 221 (1983).
[19] C. Gregoire *et al.*, Phys. Lett. B **127**, 308 (1983).
[20] F. Sebille *et al.*, Nucl. Phys. A **420**, 141 (1984); Z. Phys. A **310**, 99 (1983).
[21] T. Otsuka *et al.*, Phys. Lett. B **121**, 106 (1983).
[22] J. Wilczynski *et al.*, Nucl. Phys. A **373**, 109 (1982).
[23] M. K. Sharma *et al.*, Nucl. Phys. A **776**, 83 (2006).
[24] L. Corradi *et al.*, Phys. Rev. C **71**, 014609 (2005).
[25] M. Das Gupta, P. R. S. Gomes, D. J. Hinde, S. B. Moraes, R. M. Anjos, A. C. Berriman, R. D. Butt, N. Carlin, J. Lubian, C. R. Morton, J. O. Newton, and A. Szanto de Toledo, Phys. Rev. C **70**, 024606 (2004).
[26] S. Chakrabarty, B. S. Tomar, A. Goswami, G. K. Gubbi, S. B. Manohar, A. Sharma, B. B. Kumar, and S. Mukherjee, Nucl. Phys. A **678**, 355 (2000).
[27] M. Cavinato, E. Fabrici, E. Gadioli, E. Gadioli Erba, P. Vergani, M. Crippa, G. Colombo, L. Redaelli, and M. Ripamonti, Phys. Rev. C **52**, 2577 (1995).
[28] D. J. Parker, J. J. Hogan, and J. Asher, Phys. Rev. C **39**, 2256 (1989).
[29] P. P. Singh, B. P. Singh, M. K. Sharma, Unnati, D. P. Singh, R. Kumar, K. S. Golda, and R. Prasad, Phys. Rev. C **77**, 014607 (2008).
[30] D. J. Parker, J. Asher, T. W. Conlon, and N. Naquib, Phys. Rev. C **35**, 161 (1987).
[31] M. K. Sharma *et al.*, Phys. Rev. C **75**, 064608 (2007).
[32] P. P. Singh, M. K. Sharma, Unnati, D. P. Singh, R. Kumar, K. S. Golda, B. P. Singh, and R. Prasad, Eur. Phys. J. A **34**, 29 (2007).
[33] S. Sodaye, K. Sudarshan, B. S. Tomar, A. Goswami, S. Mukherjee, and K. Mehta, Eur. Phys. J. A **14**, 371 (2002).
[34] N. Added, R. M. Dos Anjos, N. Carlin, L. Fante Jr., M. C. S. Figueira, R. Matheus, E. M. Szanto, and A. Szanto de Toledo, Nucl. Phys. A **540**, 328 (1992).
[35] B. S. Tomar, A. Goswami, A. V. R. Reddy, S. K. Das, P. P. Burte, S. B. Manohar, and B. John, Phys. Rev. C **49**, 941 (1994).
[36] B. S. Tomar, A. Goswami, G. K. Gubbi, A. V. R. Reddy, S. B. Manohar, B. John, and S. K. Kataria, Phys. Rev. C **58**, 3478 (1998).
[37] R. I. Badren, D. J. Parker, and N. Naquib, Eur. Phys. Rev. J. A **12**, 317 (2001).
[38] Unnati, P. P. Singh, D. P. Singh, M. K. Sharma, A. Yadav, R. Kumar, K. S. Golda, B. P. Singh, A. K. Sinha, and R. Prasad, Nucl. Phys. A **811**, 77 (2008).
[39] M. K. Sharma *et al.*, Phys. Rev. C **70**, 044606 (2004).
[40] D. P. Singh, Unnati, P. P. Singh, A. Yadav, M. K. Sharma, R. Kumar, K. S. Golda, B. P. Singh, A. K. Sinha, and R. Prasad, Phys. Rev. C **80**, 014601 (2009).
[41] FREEDOM, data acquisition and analysis system designed to support the accelerator-based experiments at the Nuclear Science Centre, New Delhi, India.
[42] E. Browne and R. B. Firestone, *Table of Radioactive Isotopes* (Wiley, New York, 1986).
[43] Devendra P. Singh, Ph.D. thesis, Aligarh Muslim University, Aligarh, India, 2010.
[44] S. F. Mughabghab, M. Divadeenam, and N. E. Holden, *Neutron Cross Sections* (Academic Press, New York, 1981), Part A, Vol. 1, p. 89.
[45] J. F. Ziegler, J. P. Biersack, and U. Littmark, *Stopping and Range of Ions in Matter* (Pergamon Press, New York, 1985).